Honors Thesis:

Monte Carlo Study of a Level II Trigger Cut for the K0TO Experiment

By

Celeste Carruth

Submitted to the University of Michigan in partial fulfillment
of graduation requirements for Honors in the degree of Bachelor of Science in Physics

Department of Physics
University of Michigan
March 2013

Advisor: Myron Campbell

ABSTRACT

The K0TO experiment will use a high intensity proton beam at the Japan Proton Accelerator Research Complex (J-PARC) to study the rare decay $K_L \rightarrow \pi^0 \nu \bar{\nu}$. The goals of the experiment are to study CP violation in the quark sector, measure certain parameters of the Standard Model, and search for new physics beyond the Standard Model. This decay has a branching ratio of $2.43 * 10^{-11}$ [1], which requires the two levels of live trigger cuts in the data acquisition (DAQ) system to quickly identify and reject large percentages of background events. The original plan for the level II trigger cut proved to be impossible to perform in the current DAQ system, so an alternative idea for the cut, a threshold based on the center of energy distribution in the primary detector, was proposed by Professor Myron Campbell. Initial Monte Carlo simulation studies of the center of the center of energy distribution indicated that it is an effective method for separating background events from our signal event. Subsequent research on the effectiveness of the cut with relation to both the level I trigger cut and the uncertainty in the energy signals from the crystals confirms that this cut will satisfy the event rate limitations of the DAQ system while rejecting only a minimal number of signal events.

ACKNOWLEDGMENTS

This thesis would not have been possible without the guidance and help of many individuals who have encouraged me to study physics, provided me the opportunity to perform research, answered my questions, and continually supported me in my gradual decision to pursue a career as a physicist.

First and foremost, I would like to thank Professor Myron Campbell, who hired me as a lab assistant in the K0TO group only a few days after I started college and has been a mentor to me ever since. He has given me opportunities to work on many aspects of the project, both at the University of Michigan and at J-PARC, and encouraged me to work on the simulation studies that are now the focus of this thesis. The hours he spent teaching me as I worked on hardware and research projects have had a great impact on my understanding of physics research and my desire to pursue a career as a physicist.

Professor Jean Krisch, my academic advisor in physics, has devoted a remarkable amount of time to answering my questions about physics and encouraging me to take the classes I would need in order to study physics in graduate school, even during my first few semesters when I was planning to become a professional violinist instead. I will forever be grateful for her continual encouragement to pursue physics as a career, and, in particular, for her help with my graduate school applications.

Dr. Monica Tecchio helped me the most in the formative stages of the research for this project. She set up the framework for the center of energy study, introduced me to ROOT software, and has helped me navigate the challenges of systematically studying the simulated data. Jon Ameel, the electronics shop manager, taught me how to solder and helped teach me how to design and manufacture hardware devices to work with electronics. Professor Hajime Nanjo from Kyoto University was also extremely helpful by answering my questions about the Monte Carlo simulation framework, and also taught me some elements of detector design as I worked with him to install detectors at J-PARC prior to a test beam run. Postdoctoral fellows Koji Shiomi and Shumin Li, and graduate students Jia Xu, Yasuyuki Sugiyama, and Kazufumi Sato were also very helpful in answering my questions while I learned how to work with ROOT software and C++. I am also extremely grateful to Professor Takeshi Komatsubara from KEK for coordinating many of the details associated with my summer work in Japan.

I also owe my thanks to the many violin teachers who helped me develop the discipline and patience that are necessary for success in both physics and music. Many of these teachers have donated their time to help me as I worked to become a violinist. Although I no longer plan to pursue music as a full-time career, I will always enjoy opportunities to play music as occasions arise. I also know that that the technical acuity I have developed in my fingers will continue to be useful in my career as an experimental physicist.

Finally, I would like to thank my parents, Brent and LaJean Carruth, and my older brother and sister Nathan and Amy. My parents homeschooled me for eleven years, during which time they taught my siblings and me to ask questions, explore natural phenomena, and enjoy life. I am grateful for my family's support in my decision to pursue physics in graduate school, just as they have supported me in studying the violin.

Contents

Chapter 1

Introduction

The K0TO experiment is designed to study the rare decay $K_L \to \pi^0 \nu\bar{\nu}$. Our long-term goal is to measure around 100 events, which will allow us to determine the branching ratio with a sensitivity of $3 * 10^{-12}$, measure the height of the CKM unitary triangle, study CP violation, and search for physics beyond the Standard Model. This experiment is being conducted at the Japan Proton Accelerator Research Complex (J-PARC), in Tokai-mura, Japan, and will have its first physics run in May, June, and July 2013.

1.1 Physics Motivation for the K0TO Experiment

The asymmetry between the quantities of matter and anti-matter we observe in the universe is one of the most important topics in particle physics research. Charge parity (CP) violation in particle interactions and decays leads to this asymmetry, although our current understanding of it does not explain the extent to which matter dominates. The $K_L \to \pi^0 \nu\bar{\nu}$ decay is one of the best decays for studying this phenomenon, although studying this decay is fairly difficult due to its low branching ratio, which is on the order of 10^{-11}.

Our signal decay is a flavor changing neutral current (FCNC) process where a top quark mediates the decay of a strange quark to a down quark. Consequently, this decay provides a useful probe for studying CP violation in the quark sector. Since the decay is expected to occur via a loop process (see figure 1.1a), this event may involve physics beyond the Standard Model. Various extensions to the Standard Model suggest different branching ratios; for example, the Minimal Supersymmetric extensions of the Standard Model (MSSM) suggests that the branching ratio would be about ten times larger than the Standard Model prediction [2].

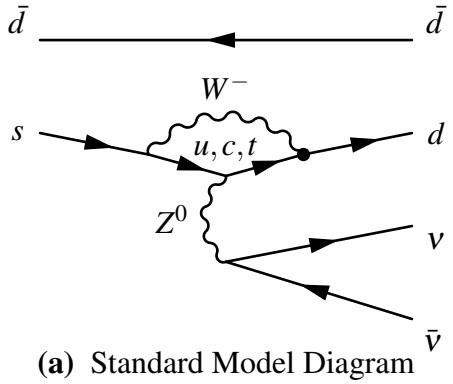

(a) Standard Model Diagram

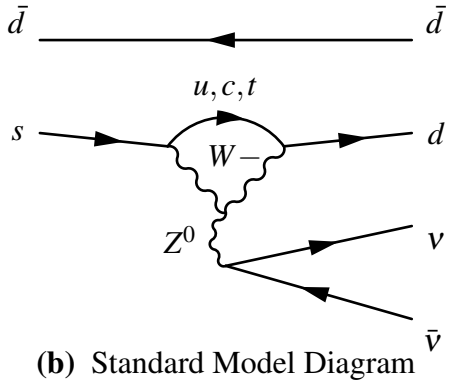

(b) Standard Model Diagram

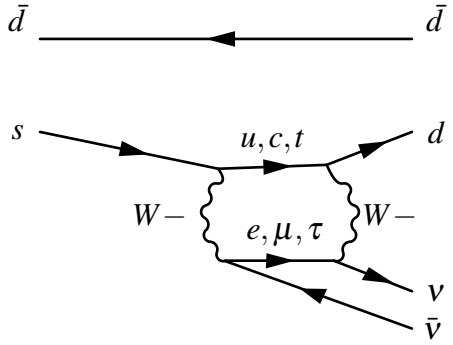

(c) Standard Model Diagram

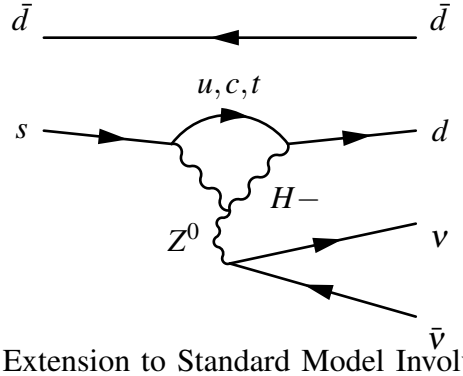

(d) Extension to Standard Model Involving Charged Higgs Boson

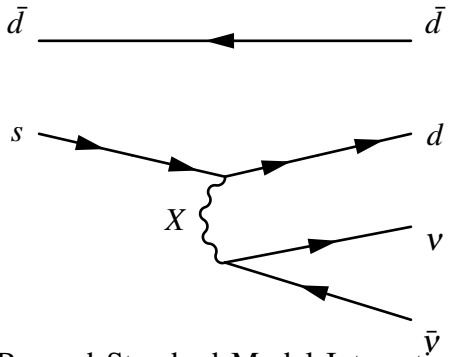

(e) Beyond Standard Model Interaction Involving Unknown Particle

Figure 1.1 Feynman Diagrams for $K_L \to \pi^0 \nu \bar{\nu}$ decays

The Cabibbo-Kobayashi-Maskawa (CKM) matrix is a 3 x 3 complex unitary matrix [3], shown in equation 1.1, with entries [4] that represent the coupling constants between different quarks.

$$V = \begin{pmatrix} V_{ud} & V_{us} & V_{ub} \\ V_{cd} & V_{cs} & V_{cb} \\ V_{td} & V_{ts} & V_{tb} \end{pmatrix} = \begin{pmatrix} 0.97428 \pm 0.00015 & 0.2253 \pm 0.0007 & 0.2253^{+0.0007}_{-0.00012} \\ 0.2252 \pm 0.0007 & 0.97345^{+0.00015}_{-0.00016} & 0.0410^{+0.0011}_{-0.0007} \\ 0.00862^{+0.00026}_{-0.00020} & 0.0403^{+0.0011}_{-0.0007} & 0.999152^{+0.000030}_{-0.000045} \end{pmatrix} \tag{1.1}$$

One goal of the K0TO experiment is to measure the height of the CKM unitary triangle. This triangle is formed according to an off-diagonal condition for the matrix: $V_{us}^* V_{ud} + V_{cs}^* V_{cd} + V_{ts}^* V_{td} = 0$. By choosing one of the three products to lie along the real axis and normalizing its length to 1, the vectors form a unitary triangle in the complex plane, with height determined by the measurements for the numbers. This triangle is shown in figure 1.2:

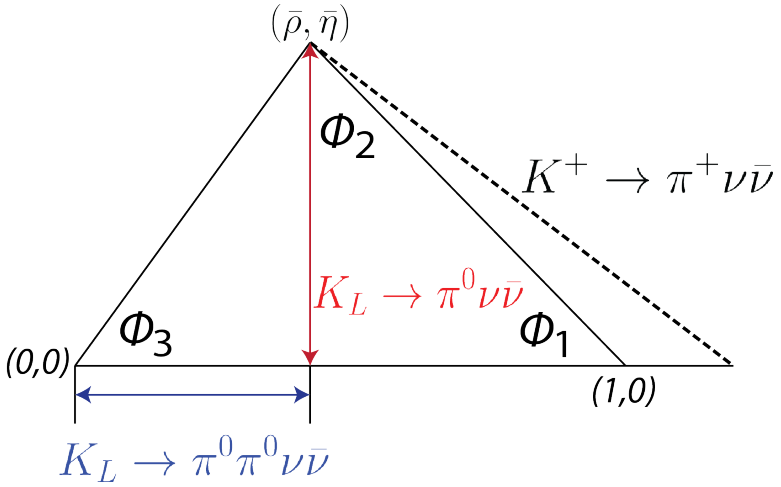

Figure 1.2 Kaon Unitary Triangle

Our signal decay is a weak interaction that involves the decay of a strange quark into a down quark, which is mediated by a W^- boson and either an up, charm, or top quark. The rate at which each process occurs is proportional to the product $V_{is}^* V_{id} * \frac{m_i^2}{m_w^2}$, for *i*= *u, c,* or *t.* Since $\frac{m_c^2}{m_w^2} \approx 2.5 * 10^{-4}$, $\frac{m_u^2}{m_w^2} \approx 9.8 * 10^{-10}$, and $\frac{m_t^2}{m_w^2} \approx 172/80 = 2.15$, the decay the K0TO experiment studies is dominated by the top quark, and thus the experiment will be sensitive to the $V_{ts}^* V_{td}$ product. The amplitude of the $K_L^0 \to \pi^0 \nu\bar{\nu}$ decay is then proportional to the imaginary part of the product, $Im(V_{ts}^* V_{td})$, which corresponds to the height of the triangle.

1.2 $K_L \to \pi^0 \nu\bar{\nu}$ Branching Ratio

Theoretical Expectation for Branching Ratio

The branching ratio is calculated to be [1]

$$B(K_L^0 \to \pi^0 \nu\bar{\nu}) = (2.20 \pm 0.07) \times 10^{-10} \left(\frac{\lambda}{0.2248} \right)^8 * \left[\frac{Im(V_{ts}^* V_{td})}{\lambda^5} * X(x_t)^2 \right] \quad (1.2)$$

In this equation, λ=$|V_{us}|$, $X(x_t)$=1.464$\pm$0.041 is the value of Inami-Lim loop function [5], and x_t is the ratio of the masses of the top quark and W boson. This gives us a branching ratio of $(2.43 \pm 0.06) * 10^{-11}$ [6], with a theoretical uncertainty of only 1-2% [7]. By measuring at least 100 events, we will determine the branching ratio with a sensitivity of $3 * 10^{-12}$. Since the theoretical uncertainty is so small, a measured branching ratio that differs significantly from the Standard Model value would be strongly indicative of an interaction involving physics beyond the Standard Model.

Expectations from Previous Experiments

During the first physics run in May-July 2013, the K0TO experiment will reach the Grossman-Nir limit. This is a limit based on the ratio of the branching ratios of $K_L \to \pi^0 \nu\bar{\nu}$ and $K^+ \to \pi^+ \nu\bar{\nu}$. Experiments E787 and E949 at Brookhaven National Laboratory have measured the branching ratio of the $K^+ \to \pi^+ \nu\bar{\nu}$ decay to be $14.7^{+13.0}_{-8.9} * 10^{-11}$ [8], which means we can expect the branching ratio for $K_L \to \pi^0 \nu\bar{\nu}$ events to be less than $1.5 * 10^{-9}$. Experiment E391a at KEK searched for $K_L \to \pi^0 \nu\bar{\nu}$ events and concluded that the branching ratio is less than $6.7 * 10^{-8}$ [9]; the K0TO experiment will be the first to reach the Grossman-Nir limit for $K_L \to \pi^0 \nu\bar{\nu}$ events. The Grossman-Nir limit and branching ratio predictions from the Standard Model and theories beyond the Standard Model are shown in figure 1.3:

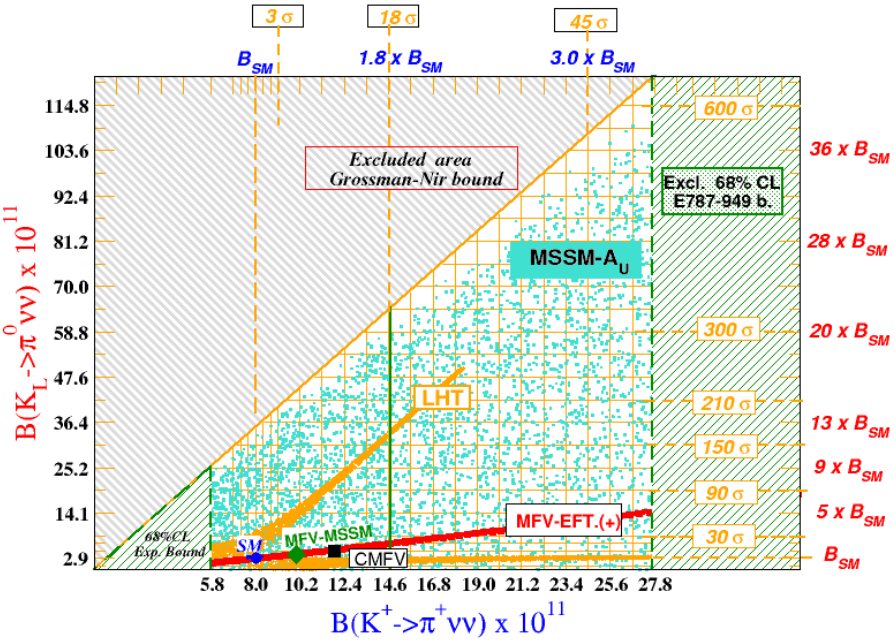

Figure 1.3 The Grossman-Nir Limit, image courtesy of [8]

1.3 Identifying Background and Signal Events

Background events consist primarily of other kaon decay channels, and come in two flavors: charged and neutral. There is also a neutron background in the beam, but it is suppressed by collimators along the beamline. Most of the decays with a charged particle, such as an electron, are, ideally, rejected by the level 1 trigger cut, since the charged particle detectors cover the entire decay region and the detectors are designed to have a high sensitivity. Our signal event, $K_L \to \pi^0 \nu\bar{\nu}$, is the only neutral event with neutrinos; all neutral background events decay exclusively into photons. Differentiating between neutral background events and our signal event in the level 2 trigger stage has proven to be a rather challenging problem.

The original plan for the level 2 trigger cut was to implement a clustering algorithm that would search for clusters of energy in the CsI crystals. However, as the DAQ system was developed, it became clear this method would be prone to miscounting the number of clusters, and, consequently, include the risk of rejecting signal events. At this stage in the data acquisition system, information from different CsI crystals is still distributed between several crates of ADC boards and level 2 trigger boards. It would be relatively straight forward to search for a cluster of energy in discrete sections of crystals, since a section of 256 crystals is mapped to a single level 2 trigger board, but this would ignore or miscount

any energy clusters that span two or more sections.

An example of this scenario is shown in figure 1.4, where the grid squares represent crystals, the black dot shows the hit position of the photon, and the color of the squares represents the amount of energy deposited in each crystal. At the level 2 stage, there is no single board that has the full picture of the energy distribution, so there is no reliable way to implement this clustering algorithm. Consequently, we needed a new plan for the level 2 trigger cut.

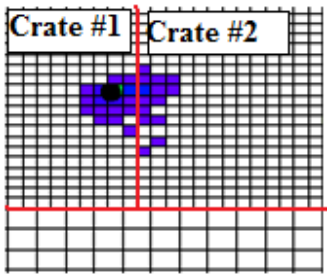

Figure 1.4 Photon Energy Cluster Mapped to Different Crates

One important characteristic of our signal event is that although it is a three-body decay, the neutrino and antineutrino are undetected but carry away a significant amount of momentum. Consequently, we expect that the pion, which immediately decays into two γ-rays, will have a large amount of transverse momentum. This means that the photons will travel off to one side, rather than being oriented around the origin. In the neutral background events, though, there are no neutrinos involved, so there will be no "missing" energy.

The reconstructed transverse momentum of the π^0 in $K_L \to \pi^0 \nu \bar{\nu}$ events is one of the requirements for events that will be accepted into our final data set. The reconstruction algorithm requires the mass of the pion to be equal to the four momenta of the two photons:

$$\begin{aligned} m_{\pi^0}^2 &= (p_1^\mu + p_2^\mu)^2 \\ &= p_1^\mu p_1^\mu + p_2^\mu p_2^\mu + 2 p_1^\mu p_2^\mu \\ &= 2(E_1 E_2 - \mathbf{p_1} \cdot \mathbf{p_2}) \\ &= 2E_1 E_2 (1 - cos\theta) \end{aligned}$$

Figure 1.5 illustrates the reconstruction method for using the energy and position of the photons to determine the decay vertex of the π^0, given the mass of the π^0. The law of cosines relates the different parameters: $r_{12}^2 = d_1^2 + d_2^2 - 2d_1 d_2 \times cos\theta$. Note that we cannot perform reconstruction algorithms at the level 2 trigger stage because, as previously discussed, no single circuit board has the full picture of energy clusters in the CsI crystals.

The box in figure 1.6 shows the "signal" region for $K_L \to \pi^0 \nu \bar{\nu}$ events. In order to improve the signal to noise ratio as much as possible, it was decided that the final data set will only include events where the reconstructed π^0 vertex along the z axis is between three and five meters and the reconstructed π^0 transverse momentum (Pt) is between 1.30 and 2.5 GeV/c. Since we do not detect the neutrinos, the transverse momentum for the single π^0 becomes the net transverse momentum that we measure. This is quite different from background events where the detectors can detect all of the end decay products, and consequently the sum of the transverse momenta of all particles in background events is close to zero.

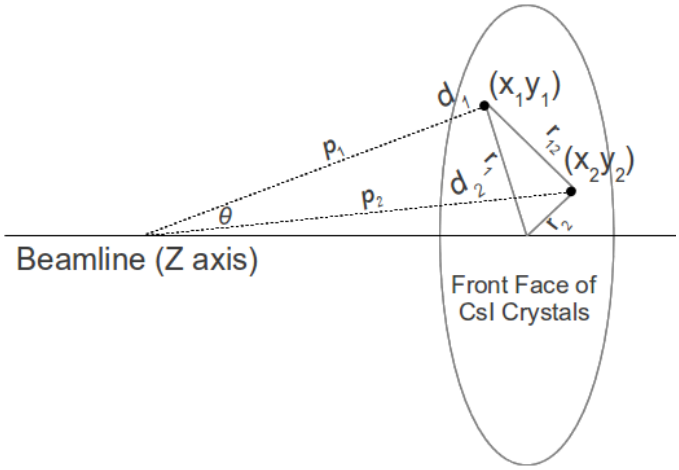

Figure 1.5 π^0 decay vertex reconstruction from two γs.

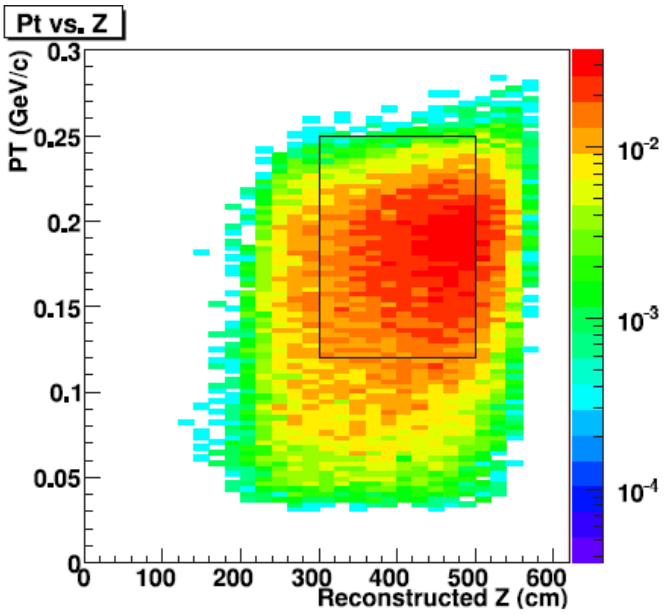

Figure 1.6 Distribution of the transverse momentum versus reconstructed decay vertex along the z axis for the π^0 in signal events, with the signal region indicated by the rectangle. Image courtesy of [10].

Background Events

Several of the most important background decay channels are listed in table 1.1. These decays either have the largest branching ratios or have end decay products that are similar to those in our signal event.

Table 1.1 Background Decays

Background Event	**Branching Ratio [4]**
$K_L \to \pi^{\pm} e^{\mp} \nu_e$	$(40.55 \pm 0.12)\%$
$K_L \to \pi^{\pm} \mu^{\mp} \nu_\mu$	$(27.04 \pm 0.07)\%$
$K_L \to \pi^0 \pi^0 \pi^0$	$(19.52 \pm 0.12)\%$
$K_L \to \pi^{\pm} \pi^{\mp} \pi^0$	$(12.54 \pm 0.05)\%$
$K_L \to \pi^0 \pi^0$	$(8.65 \pm 0.06) * 10^{-4}$
$K_L \to \gamma\gamma$	$(5.47 \pm 0.04) * 10^{-4}$

Possible Method for Rejecting Background Events

The level I trigger cut will generally accept neutral background events where all photons hit the CsI crystals. Because neutral background events decay exclusively into photons, not neutrinos, in an event where every photon hits the CsI crystals, the net transverse momentum of will be near zero for background events and relatively large for signal events. As a result, the center of energy deposited in the crystals is near the origin for background events, but at some distance from the origin in signal events, as shown in figure 1.7.

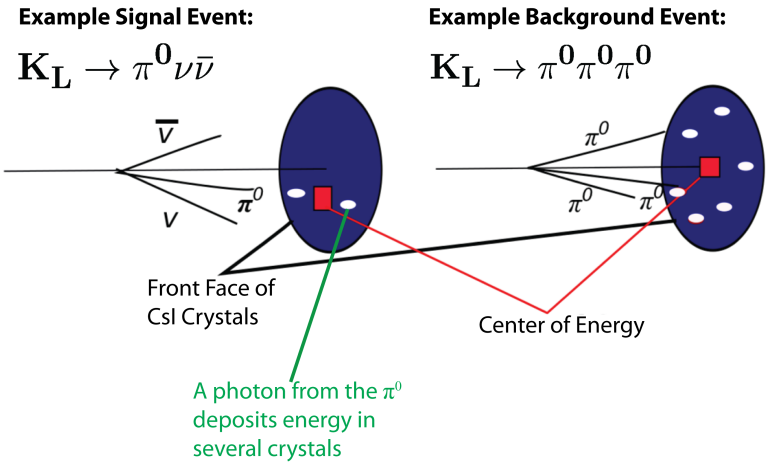

Figure 1.7 Potential Center of Energy Cut

Professor Myron Campbell suggested that this difference in the center of energy distributions could provide a way to differentiate between signal and background events at the

level 2 trigger stage. Since the center of energy is essentially a sum of the energy detected by a crystal multiplied by its position in the x-y plane, this can be calculated in sections and then summed together at the end. Monte Carlo simulation studies of the center of energy distributions for signal and background events are the focus of this thesis.

1.4 Center of Energy Calculation

The center of energy (CoE) calculation uses the following equation, where the index i represents an individual crystal:

$$\frac{\sqrt{\left(\sum_{i=1}^{2716} E_i x_i\right)^2 + \left(\sum_{i=1}^{2716} E_i y_i\right)^2}}{\sum_{i=1}^{2716} E_i} \tag{1.3}$$

This gives a result in units of length, which, as will be discussed later, is generally less than 13 cm for background events and greater than 13 cm for $K_L \to \pi^0 \nu \bar{\nu}$ events.

Chapter 2

K0TO at J-PARC

2.1 Detector Setup

The detectors are installed in Hadron Hall at J-PARC. The decay region is completely enclosed by photon and charged particle detectors, which are made of scintillating materials. When a photon or charged particle interacts with a scintillator, the scintillator emits electromagnetic radiation, which is collected by photomultiplier tubes (PMTs). The photomultiplier tubes convert the flux of photons into analog energy signals, which are then preamplified and transmitted to the ADC boards in the data acquisition system.

An array of 2716 cesium iodide (CsI) crystals forms a calorimeter that measures the energy and positions of photons. CsI crystals are particularly useful for detecting γ-rays because the nuclei of the atoms are quite heavy, providing a relatively large cross-section for interactions. The nuclei are still stable, though, so they will not spontaneously emit radiation. These crystals were previously used in the KTeV experiment at Fermilab several years ago [10].

The remaining detectors that surround the decay region serve as veto detectors, because they will detect any charged particles or photons that do not hit the CsI calorimeter. We want to save events if we detect photons only in the CsI crystals and no other particles in any other detector. In order to accomplish this, energy over a certain threshold in any of the veto detectors will cause the data acquisition system to reject the event, hence the name "veto" detector. An overview of the physical locations of detectors at J-PARC is shown in figure 2.1.

The purpose of the veto detectors is to allow us to quickly and correctly identify events with charged particles and events where one or more photons do not interact with the CsI crystals. There are several collar counters (CC) that are strategically placed to detect photons going off to the side or on the inner perimeter of the CsI crystals. These are the CC01, CC02, CC03, CC04, CC05, and CC06 detectors shown in figure 2.1. The front barrel (FB) and main barrel (MB) are also photon detectors, and surround about seven meters of beam line. They cover the region between the metal target and the CsI calorimeter, and extend

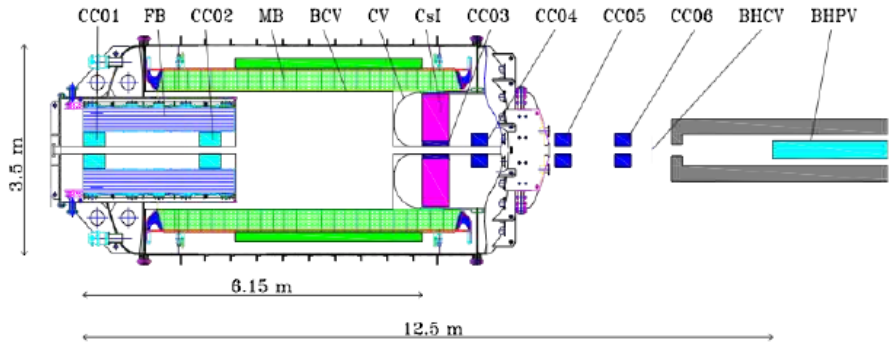

Figure 2.1 K0TO Detectors at J-PARC. Image courtesy of [10].

a short distance beyond the crystals. The barrel charge veto (BCV) and charge veto (CV) are charged particle detectors that surround the decay region and cover the front face of the CsI crystals, respectively, while the beam hole photon veto (BHPV) and beam hole charge veto (BHCV) detect photons and charged particles that travel down the beam line. The CsI and CC03 crystals are 50 cm long and are arranged according to figure 2.2.

When a photon hits one of the CsI crystals, an electromagnetic shower is induced, and energy spreads to neighboring crystals. The CC03 crystals on the inner perimeter and the main barrel on the outer perimeter are designed to detect any energy leakage, which can occur if a photon hits near the inner or outer edge. The CsI crystals are 50 cm long in order minimize the amount of energy that leaks through the back end of the crystals. With information from the CsI calorimeter and the veto detectors, we can confidently determine whether or not the photons from an event deposited all of their energy in the CsI crystals, as well as whether there were any charged particles in an event.

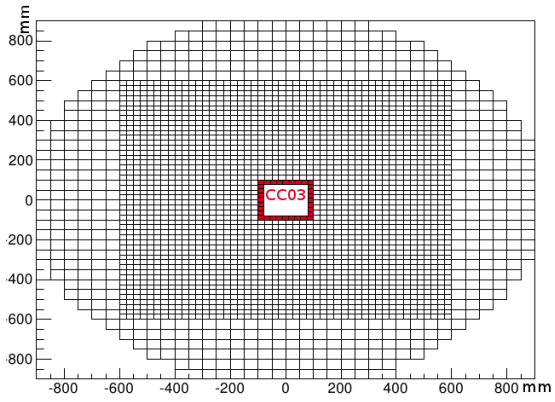

Figure 2.2 CsI Calorimeter and CC03 Detector. Image Courtesy of [10].

2.2 The Data Acquisition System

2.2.1 Overview

The data acquisition (DAQ) system consists of several sets of circuit boards that perform two levels of trigger cuts on live data, and then send the information for events that pass the level 2 cut to a computer cluster to be stored and further analyzed. The K0TO group here at the University of Michigan is the primary group responsible for these electronics. Figure 2.3 shows the layout of the system:

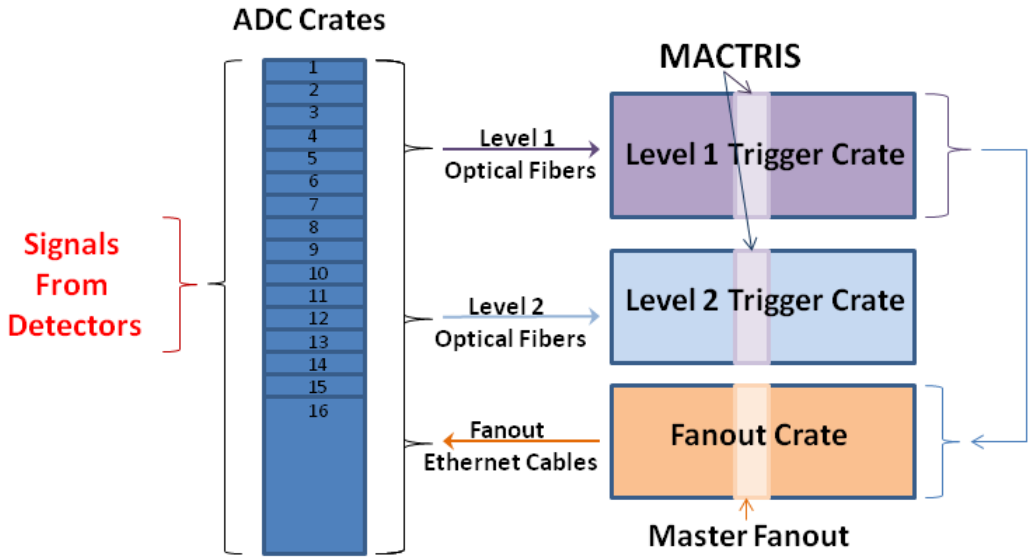

Figure 2.3 Layout of the DAQ System

The function of each board is summarized in table 2.1. These circuit boards reside in VME crates, which have backplanes that provide both power to the boards and connections for boards within a crate to communicate with each other. For example, a MACTRIS board can send the same signal to all the other boards in its crate, and level 2 boards can add up numbers from each board and send the result down the backplane to the MACTRIS board. A combination of optical fiber and ethernet cables connect boards in different crates.

In order to measure 100 $K_L \to \pi^0 \nu \bar{\nu}$ events, we need a high flux of kaons. This means that the DAQ system must operate at extremely high rates and safely remove as many background events as possible without rejecting more than a minimal number of signal events. The incoming rate of ADC events is determined by the intensity of the beam, but the level 1 trigger cut is designed to reduce the event rate to approximately 100 kHz, and the level 2 trigger cut is expected to further reduce the event rate to 5-10 kHz. Information for the events that are accepted by both the level 1 and level 2 trigger cuts is then sent to a computer cluster, Mandolin, which saves the data, searches for clusters of energy in

Table 2.1 Description of Boards Used in the DAQ System

Board	**Description**
ADC (Analog to Digital Converter) Boards	Each board has sixteen channels that accept analog signals from 16 photomultiplier tubes. They convert these analog signals to 14-bit digital signals every 8 ns and send them via separate optical fibers to the Level 1 and Level 2 Trigger boards. Each ADC board also receives clock and control signals from a fanout board.
Level 1 Trigger Boards	Each board receives energy sums from 16 ADC boards and calculates a new sum over the 16 boards, which includes 256 detector channels. These boards reside together in a single VME crate, and use daisy-chain signals over the VME backplane to calculate the total energy in different detectors. These energy sums are compared with thresholds in the MACTRIS board, which is in the middle of the VME crate.
Level 2 Trigger Boards	If the level 1 trigger accepts an event, the data will be sent from the ADCs to the level 2 trigger boards, which will then calculate the center of energy in the CsI crystals, a value that is used for the level 2 trigger decision.
MACTRIS (Master Control and Trigger Supervisor) Board	There are MACTRIS boards in both the level 1 and level 2 VME crates. They issue a clock signal, send the LIVE signal when the beam is on, and make the level 1 and level 2 decisions.
Fanout Boards	Fanout boards come in two flavors: master fanout and slave fanout. If the MACTRIS board in the level 1 crate accepts an event, it will issue a command to the master fanout, which will in turn command the slave fanout boards to tell each of the ADC boards to send the information from that event to the level 2 trigger boards.

the CsI crystals, and calculates the photons' hit positions and energies. Mandolin studies information from veto detectors that are not included in the level 1 decision and analyzes the combined information prior to assembling the final data set of $K_L \to \pi^0 \nu \bar{\nu}$ events.

2.2.2 Front End Electronics

Each channel of a detector is connected to a photomultiplier tube, which generates electrons proportional to the strength in the optical signal. The signal, now an electrical current, is then sent through a preamplifier, and from there to an ADC board. The number of ADC boards used is determined by the number of inputs in level 1 trigger boards. We plan to use 256 ADC boards in our physics run in May, so we will be able to connect to a combined total of 4096 detector channels, 2716 of which will be used by the CsI crystals. Each signal from a detector arrives as an analog signal, which the ADC board converts to a gaussian shaped signal, and digitizes it via a 14-bit 125 MHz Analog-to-Digital Converter. For the level 1 trigger system, the ADC boards will send the energy sum of the 16 input channels; for the level 2 trigger system, they will send the complete digitized energy information of the full gaussian curve for each channel.

2.2.3 Trigger System

Level 1

The level 1 trigger is activated when the total energy in the CsI crystals is above a certain threshold. This threshold will be at least the mass of a pion, 135 MeV, although probably much higher, closer to 250 MeV. When this trigger is activated, the level 1 trigger boards check the total energy levels in particular veto detectors, such as the charge veto, barrel charge veto, main barrel, front barrel, and collar counters, as shown in figure 2.1. The beam hole photon and charge veto detectors might be excluded in this stage, due to high rates of kaon interactions, although information from both detectors will be included in the offline analysis. If the energy in any of the veto detectors is above the threshold value programmed in the MACTRIS board, then the event will be ignored and the system will study the next event. The precise threshold values are yet to be determined and will be calculated following more analysis of simulated events and calibration events from real data. If all the energies in the particular veto detectors are below the threshold values, then the level 1 trigger will accept the event. In this case, a signal will be sent to the master fanout board, which then tells each of the ADC boards to send the information about the event to the level 2 trigger boards.

Level 2

If the level 1 trigger system accepts an event, data for the event will be sent via an optical link from the ADC boards to the level 2 crate, which will then calculate the center of energy

radius in the CsI crystals. Since the level 2 trigger boards are contained in a single crate, the center of energy radius calculation is completed in a daisy-chain calculation that starts at opposite ends of the crate and is summed together in series as the signal travels to the center of the crate, where the MACTRIS board will calculate the complete sum. If the center of energy radius is above the threshold value programmed in the MACTRIS board, then the level 2 trigger system will accept the event. After a decision to accept an event is issued, information from all of the detectors will be sent from the level 2 boards to a computer cluster, Mandolin, to be processed and stored.

2.2.4 Readout

Events that pass the level 2 trigger cut will be read out by and analyzed by Mandolin. All of the level 2 trigger boards are connected to Mandolin, which builds events by matching together all the data from different boards by their timing information. After building events, it can see an entire picture of the energies in each crystal and is therefore capable of completing the clustering analysis that the level 2 trigger cut is unable to perform. It searches for clusters of energy and uses that information to reconstruct which types of particles were present, as well as their energies, momenta, and decay vertices. Mandolin then compiles all of the information for an event into a single file, which is then stored for later processing. Mandolin has approximately 40 nodes, and each node has a 750 Gb and a 2 Tb disk, which provide approximately 110 Tb of temporary storage. Thirty nodes are used for a level 3 trigger cut, while 10 nodes are used for offline analysis of stored events. The level 3 trigger cut removes events depending on various parameters, such as the number of energy clusters present in the event. Once events pass the level 3 trigger cut, the event information is sent over the internet to the KEK computing cluster (KEKCC).

Chapter 3

Monte Carlo Simulation Studies

3.1 Elementary Analysis of Neutral Events

Monte Carlo simulations are computer simulations of random processes. Most particle physics experiments, including the K0TO experiment, use ROOT to run software to simulate events. The software for ROOT simulations consists of a package of files written in C or C++ code, which establish parameters for the particular decays as well as the physical characteristics of the detectors. Using Monte Carlo processes for generating random numbers provides us with a good method for studying certain characteristics of events prior to performing the actual experiment, so we were able to use simulated events to study the center of energy distributions in different decays. The simulation software for the K0TO experiment was primarily developed by Professor Hajime Nanjo from Kyoto University, and complimentary analysis software for studying and reconstructing events is currently being developed by several members of the collaboration.

In the initial study to determine whether there is a noticeable difference in the center of energy distribution of background events and signal events, we used the momentum variables generated in the Monte Carlo simulations to project photons to their expected x-y coordinates corresponding to the z coordinate plane of the CsI crystals. The first step was to study events where all photons hit within a certain region of the CsI; such events are referred to here as "fiducial" events. As an example, the black dots in figure 3.1 represent the projected hit positions of four photons from a $K_L \to \pi^0\pi^0$ event, while the colored squares represent the magnitude of the energy detected by individual crystals. In events where photons hit close to the inner or outer edge of the crystals, it is unlikely that the energy will be entirely contained in the CsI crystals. In general, if a photon hits near an edge, some energy will spill out into the CC03 and outer edge veto detectors, so these events would not be included in the final data set and were consequently eliminated from this elementary analysis. In the figure, the area between the two circles is an estimate of the fiducial area within which photons can safely deposit energy in the crystals without much leaking out to veto detectors.

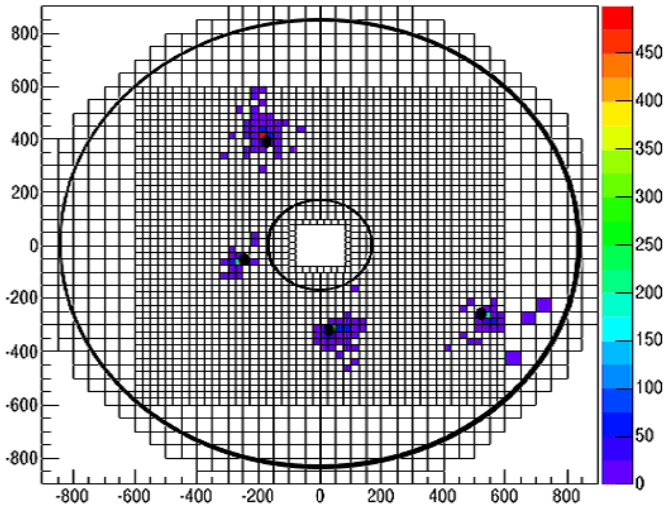

Figure 3.1 Projected Hit Positions of Photons in a Fiducial $K_L \rightarrow \pi^0\pi^0$ Event

Using this method for predicting the hit positions of photons, we studied the center of energy radius in the crystals for the signal and three background decays when all photons were expected to hit within the fiducial area. For each decay mode in this histogram, we began with approximately 500,000 simulated events and then selected the fiducial events. The results are shown in figure 3.2.

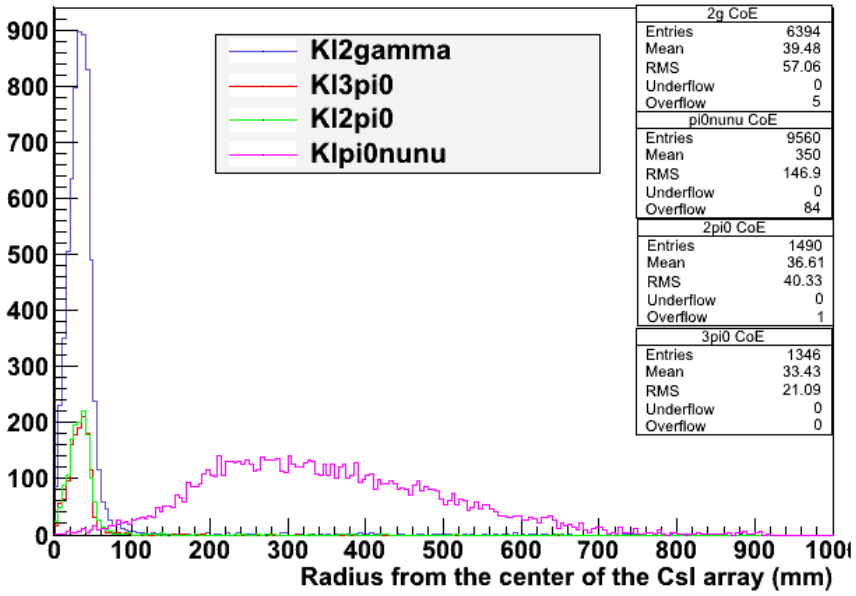

Figure 3.2 Center of Energy Radius of Fiducial Events

The branching ratios of these decays are given in table 3.1. While the histograms in figure 3.2 are not normalized by branching ratio, we can still observe that the center of energy radius in background events is generally less than the center of energy in signal events. This data provided the first analytical indication that this new idea for a cut might work.

Table 3.1 Neutral K_L Decays

Neutral Event	**Branching Ratio [4]**
$K_L \to \gamma\gamma$	$(5.47 \pm 0.04) * 10^{-4}$
$K_L \to \pi^0\pi^0\pi^0$	$(19.52 \pm 0.12) * 10^{-2}$
$K_L \to \pi^0\pi^0$	$(8.65 \pm 0.06) * 10^{-4}$
$K_L \to \pi^0\nu\bar{\nu}$	$(2.43 \pm 0.06) * 10^{-11}$

3.2 Relationship between Level 1 and Level 2 Trigger Cuts

In an ideal experiment, events pass the level 1 trigger cut only if all of the photons are fiducial, meaning that they hit within the prescribed region of the CsI crystals. If so, we would expect that this center of energy cut would be capable of removing more than 95% of background events. In reality, though, there will be many events where a photon hits a veto detector but, for some reason or other, does not deposit enough energy to bring the crystal above the threshold. We could use very low thresholds in the veto detectors to reduce this problem, but if we did, we would risk rejecting events we want to keep after performing more subtle offline analysis. Although the threshold values used in the level 1 stage will have a significant impact on the success of the level 2 trigger cut, finding the optimal values for the level 1 veto thresholds is beyond the scope of this study. Instead, we are interested in studying how the selection of level 1 veto detectors impact the effectiveness of a center of energy cut. We selected a set of threshold values, shown in table 3.2, that seemed to provide reasonably good results, and then looked at the success of level 1 and level 2 cuts with respect to the various veto detectors. In order for an event to be studied by the Level 1 trigger system, we require the total energy in the CsI calorimeter to be at least 135 MeV, the rest mass of a π^0. We also require that the energy in the veto detectors be below the threshold values in table 3.2 before an event is evaluated by the level 2 center of energy cut. The center of energy radius

Table 3.2 Theshold values used for analysis in this chapter

Detector	**Threshold (MeV)**
Charge Veto	5
Barrel Charge Veto	10
Main Barrel	15
Front Barrel	10
CC02 (now NCC)	10
CC03	15
CC04	10
CC05	10
CC06	10

used in the plots for this section is 130mm, an estimated threshold for the cut based on the number of background events with a smaller radius versus the number of signal events with a larger radius.

The center of energy distributions of background and signal events we observe in figure 3.2 is specifically for events where all photons were expected to hit within a fiducial region in the CsI crystals, a location we calculated by using variables for the momentum and decay vertex that were stored in the output ROOT file from the Monte Carlo simulations. These variables are, of course, not available in actual events, so we next modified the analysis code to include only the information we can directly access in the experiment, such as the amount of energy in a crystal and its position in the x-y plane. Table 3.4 shows us that this center of energy cut continues to be effective at removing background events when we calculate the center of energy of events only if they pass a level 1 veto cut, without any fiducial requirements on the Monte Carlo variables for the photons.

While studying the impact the veto detectors used in the level 1 veto cut have on the effectiveness of the level 2 center of energy cut in the simulated events, we wanted to address the following question: which veto detectors have the largest effect on the success of a subsequent center of energy cut, with respect to both signal and background events? It is particularly important to understand the various parameters that affect signal acceptance/rejection rates, and, although not as crucial, it is also informative to study the parameters relating to background rejection even though we plan to use most of the veto detectors in the level 1 trigger cut. We approached the question above in two different ways, for both background and signal events: we first analyzed the acceptance rate of the center of energy cut for events where we check specific veto detectors one at a time in the level 1 cut, and then we studied the acceptance rate of the center of energy cut where we include all but one veto detector in the level 1 cut.

3.2.1 Level 1 And Level 2 Cuts on $K_L \to \pi^0\pi^0\pi^0$ Events

Acceptance rates were studied for both our signal event and the most dominant background event, $K_L \to \pi^0\pi^0\pi^0$, and the results for the background analysis are summarized in tables 3.4 and 3.3, as well as represented in figures 3.4 and 3.3. While evaluating the information, it is helpful to keep in mind that it is necessary for both of the level 1 and level 2 trigger cuts to reduce event rates by factors of ten. Events considered for these acceptance studies are required to have a minimum of 135 MeV deposited in the CsI crystals. Out of one million generated events, there were 83,828 events with this energy above the threshold, which we will refer to in the following tables as "preselected" events.

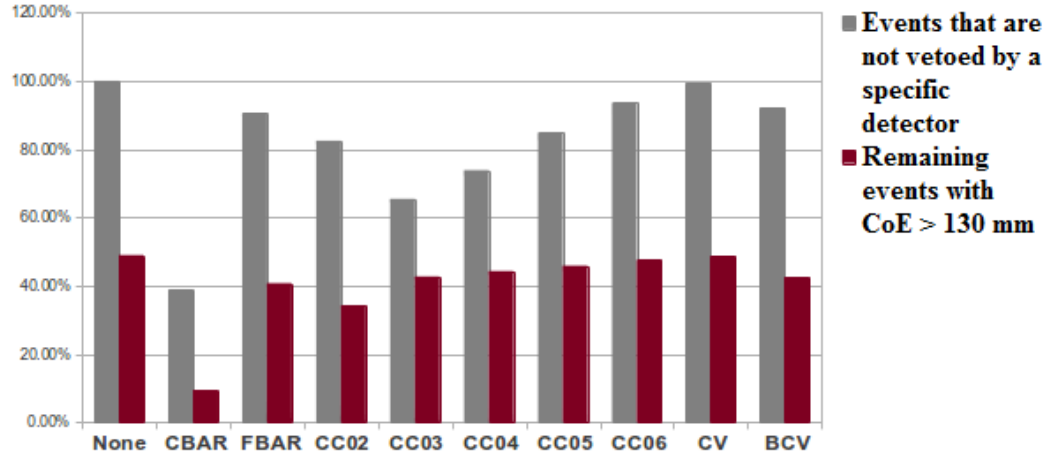

Figure 3.3 $K_L \to \pi^0\pi^0\pi^0$ Acceptance Rates of Background Events Using Individual Detectors

Table 3.3 $K_L \to \pi^0\pi^0\pi^0$ Acceptance Rates of Individual Detectors

Single Detector used as level 1 veto cut:	**Percentage of preselected events with energy below threshold in a single detector**	**Percentage of preselected events that then pass the center of energy cut**
No Detectors Included	100.0%	49.0%
Main Barrel (CBAR)	38.7%	9.5%
Front Barrel (FBAR)	90.4%	40.7%
CC02 (now NCC)	82.5%	34.2%
CC03	65.4%	42.7%
CC04	73.8%	44.3%
CC05	84.8%	45.9%
CC06	93.6%	47.6%
Charge Veto (CV)	99.4%	48.6%
Barrel Charge Veto (BCV)	92.0%	42.5%

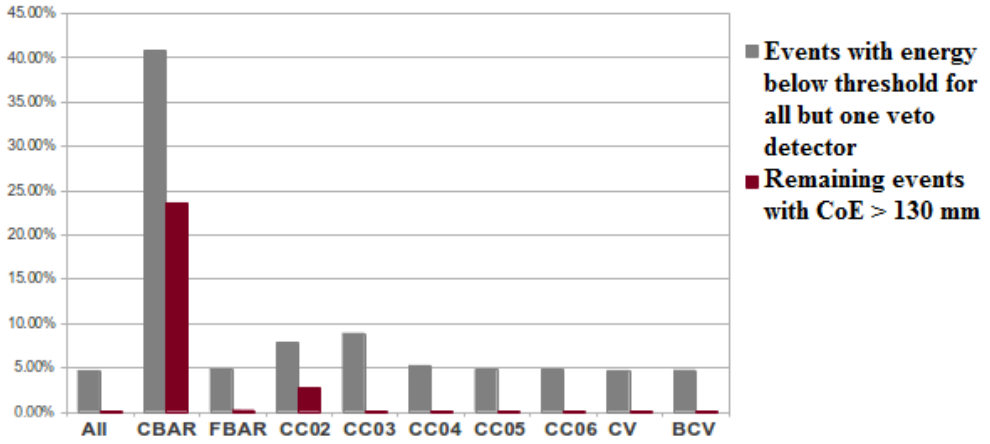

Figure 3.4 $K_L \to \pi^0\pi^0\pi^0$ Acceptance Rates of Background Events with Energy Below Threshold for All but One Detector

Table 3.4 $K_L \to \pi^0\pi^0\pi^0$ Acceptance Rates of Background Events with Energy Below Threshold for All but One Detector

Detector EXCLUDED from Level 1 veto cut	**Percentage of preselected events with energy below threshold in all other veto detectors**	**Percentage of preselected events that then pass the center of energy cut**
All Detectors Included	4.7%	0.1%
Main Barrel (CBAR)	40.8%	23.6%
Front Barrel (FBAR)	4.9%	0.2%
CC02 (now NCC)	7.8%	2.7%
CC03	8.9%	0.1%
CC04	5.3%	0.1%
CC05	4.8%	0.1%
CC06	4.8%	0.1%
Charge Veto (CV)	4.7%	0.1%
Barrel Charge Veto (BCV)	4.7%	0.1%

The acceptance rates in table 3.3 indicate that the main barrel is the single most effective detector for reducing events in the level 1 and level 2 trigger cuts, which we naturally expect because it covers the largest fraction of the decay region. Although the CC02 cut does not reject a significant number of events at the level 1 stage, it has the next largest fractional difference (after the main barrel) in the percentages of accepted events between the level 1 and center of energy cuts.

In table 3.4 we observe that when almost all the detectors are used, the acceptance rates should be sufficiently low enough to satisfy the rate limitations of the DAQ system. When all the veto detectors are used, the center of energy cut reduces events by almost a factor of ten, and lowering threshold values in the veto detectors could reduce this background acceptance rate even more. It is also apparent that the main barrel continues to have the largest effect on acceptance rates; if we remove it from the veto cut, we accept over 20% more events than if we remove any other single detector.

3.2.2 Level 1 and Level 2 Cuts on Signal Events

We must now address a more important question: would a center of energy cut reject signal events we want to keep? We approach this question using the same method as in the previous section, in figures 3.5 and 3.6 and tables 3.5 and 3.6. Unlike the data for $K_L \to \pi^0\pi^0\pi^0$ events, the data for preselected $K_L \to \pi^0\nu\bar{\nu}$ events consists only of reconstructed events. As before, events are preselected only if there is at least 135 MeV deposited in the CsI crystals. Out of one million simulated $K_L \to \pi^0\nu\bar{\nu}$ events, there were 22674 such events, which form the preselected set used in the following tables and diagrams.

The reconstruction algorithm finds clusters of energy in the CsI crystals and performs several calculations on these clusters to reconstruct the π^0's decay transverse momentum and decay vertex, which was briefly described in section 1.3. A reconstructed $K_L \to \pi^0\nu\bar{\nu}$ event must have only two energy clusters, since both photons must hit the CsI calorimeter. Although it appears that almost 30% of signal events are rejected by veto detectors, it is important to remember that additional requirements are made for the signal events that will be included in the final data set. For example, for events in our final data set, the reconstructed hit positions must be within a fiducial region. If we were to take this into consideration, we would expect that many of these events that are rejected by the CC03 detector, which collects energy leakage along the inside perimeter of the CsI crystals, would not be included in the final data set.

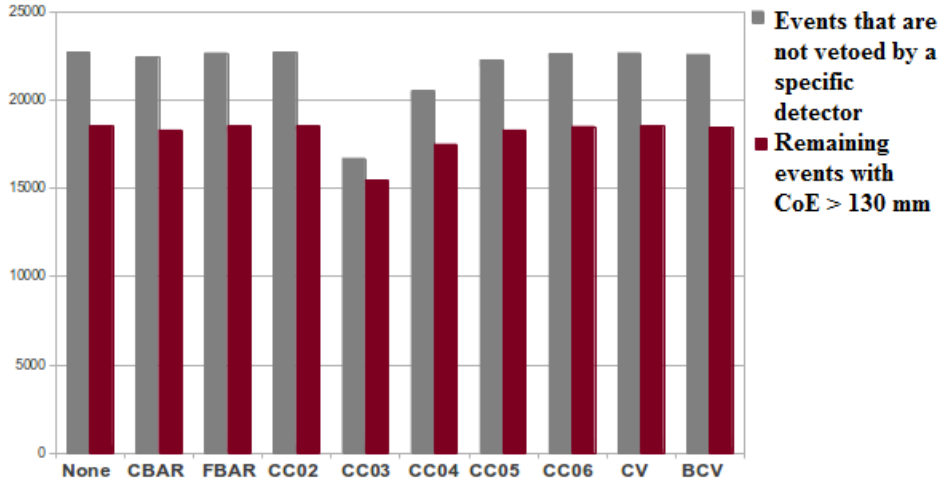

Figure 3.5 $K_L \to \pi^0 \nu \bar{\nu}$ Acceptance After Single Veto Detector Cuts and the Center of Energy Cut

Table 3.5 $K_L \to \pi^0 \nu \bar{\nu}$ Acceptance Rates of Individual Detectors

Single Detector used in Level 1 veto:	**Percentage of preselected events with energy below threshold in a single detector**	**Percentage of preselected events that then pass the center of energy cut**
No Detector Included	100%	81.8%
Main Barrel (CBAR)	98.8%	80.6%
Front Barrel (FBAR)	99.9 %	81.7%
CC02 (now NCC)	100%	81.8%
CC03	73.6%	68.1%
CC04	90.4%	77.1%
CC05	98.2%	80.7%
CC06	99.7%	81.5%
Charge Veto (CV)	99.9%	81.7%
Barrel Charge Veto (BCV)	99.5%	81.3%

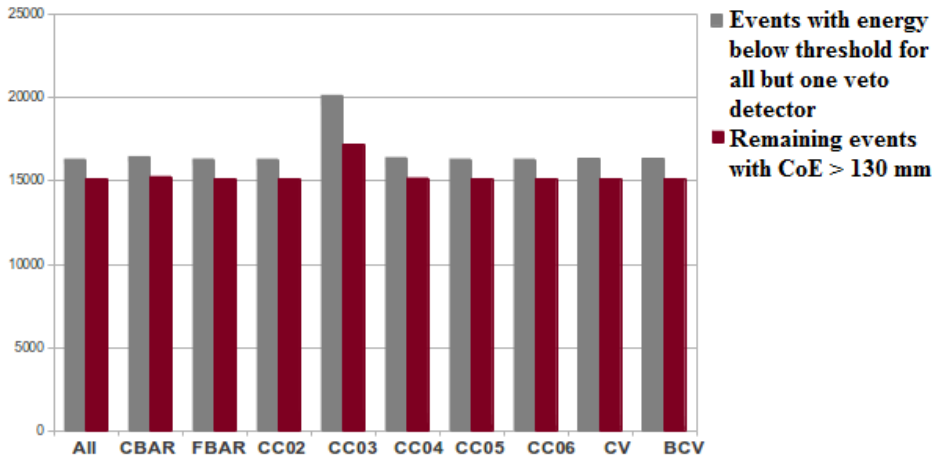

Figure 3.6 Acceptance Rates for Signal Events with Energy Below Threshold for All but One Detector

Table 3.6 $K_L \to \pi^0 \nu \bar{\nu}$ Acceptance Rates for Signal Events with Energy Below Threshold for All but One Detector

Detector EXCLUDED from Level 1 veto cut	**Percentage of preselected events that pass all the remaining threshold cuts**	**Percentage of preselected events that then pass the center of energy cut**
All Detectors Included	71.9%	66.6%
Main Barrel (CBAR)	72.6%	67.3%
Front Barrel (FBAR)	71.9%	66.7%
CC02 (now NCC)	71.9%	66.6%
CC03	88.8%	75.7%
CC04	72.3%	66.9%
CC05	71.9%	66.7%
CC06	71.9%	66.7%
Charge Veto (CV)	72.0%	66.7%
Barrel Charge Veto (BCV)	72.0%	66.7%

We observe in the data above that the CC03 detector rejects the most signal events. To better understand how the threshold in this detector affects acceptance rates, we plotted the acceptance rate versus threshold value, as shown in figure 3.7.

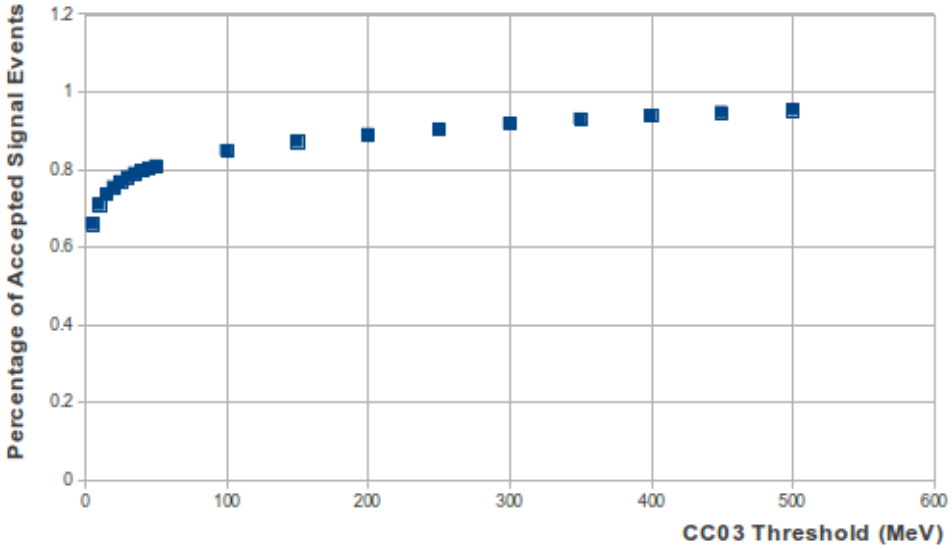

Figure 3.7 Signal Acceptance Versus CC03 Cut

We conclude that in order for the CC03 detector to accept more events, we would need to have a much higher threshold. However, even though there was enough energy in the CsI crystals to reconstruct an event, we are not very interested in these events because a significant amount of energy has leaked out into the CC03 crystals. Even if we use a larger threshold value, the combination of other detectors and the center of energy cut would still reject about 25% of the events, and the center of energy cut by itself rejects more than 18% of events. These would seem like unacceptably large percentages until we look at what type of $K_L \to \pi^0 \nu \bar{\nu}$ events are being rejected. As shown in figure 1.6, $K_L \to \pi^0 \nu \bar{\nu}$ events will only be included in the final data set if the π^0's transverse momentum and decay vertex fall within a signal region. We then plotted the reconstructed transverse momentum and decay vertex for signal events and colored them green if their center of energy was greater than 130 mm and red if it was less than 130 mm:

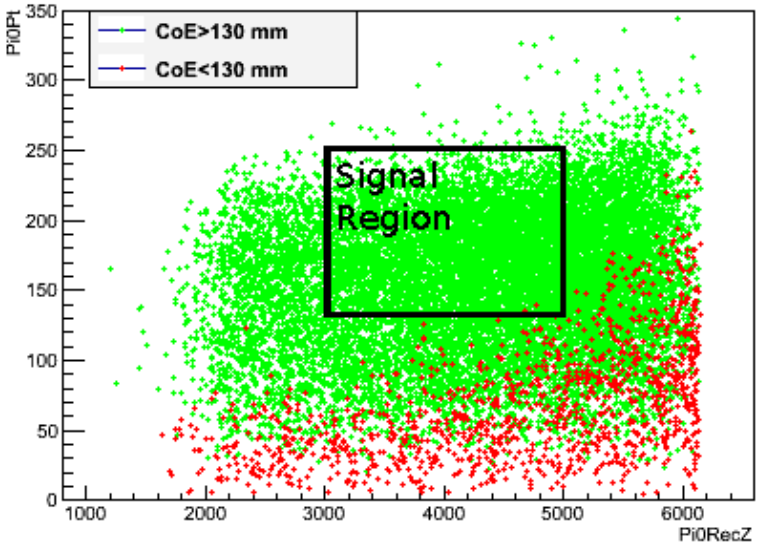

Figure 3.8 Signal Acceptance With Center of Energy Cut

We see that only a few events in the signal region, on the order of 1 per thousand, would be rejected by a center of energy cut. This gives us enough confidence that the center of energy cut is safe to implement, although we will need to carefully study the ratio of events in the signal region that are rejected and events not in the signal region that are rejected.

3.3 Effect of Random Deviations on Center of Energy Cut

Having used Monte Carlo variables that would be available to the level 2 trigger system in our live data stream, we needed to study the effects of statistical and systematic uncertainties of those variables. In particular, we considered uncertainties in the position of and the energy measured by each crystal. In an effort to see whether these deviations have a significant impact on the success of a center of energy cut, graduate student Jia Xu made the following plots, using deviations described in table 3.7.

Table 3.7 Deviations of Variables

Parameter	**Magnitude of Deviation**
Position scale (due to gap between crystals)	0.4%
Overall displacement of crystals	2 cm
Statistical distribution of calibration constants	Use average values
Energy resolution of crystals	Randomly smear the recorded energy

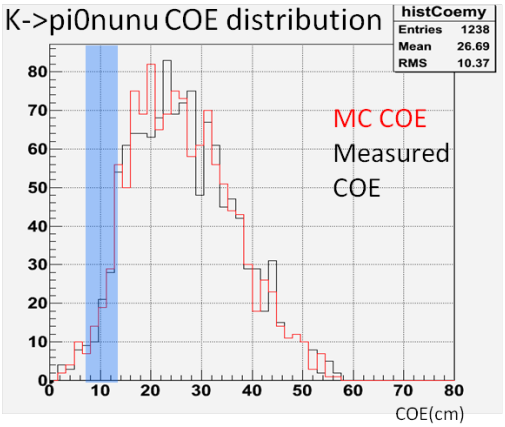

(a) Center of Energy Radius of $K_L \to \pi^0 \nu \bar{\nu}$ events

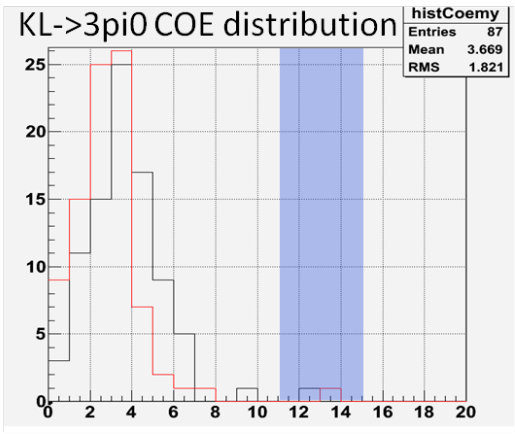

(b) Center of Energy Radius of $K_L \to \pi^0 \pi^0 \pi^0$ events

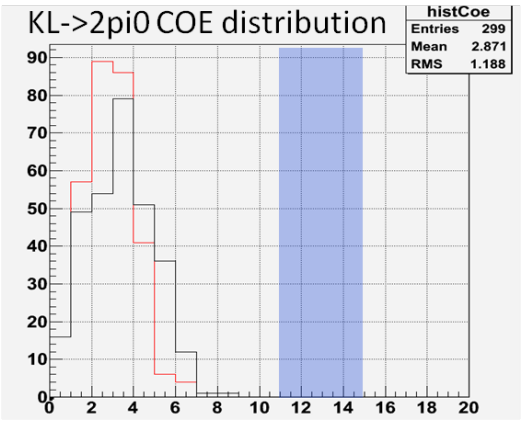

(c) Center of Energy Radius of $K_L \to \pi^0 \pi^0$ events

Figure 3.9 Center of Energy Radius With Potential Fluctuations. The red histograms correspond to the result using original Monte Carlo variables, and the black histograms correspond to the result using randomly altered variables, following the parameters in table 3.7. Images courtesy of [11].

In the figures on the previous page, the vertical blue band represents the approximate location of a center of energy cut. A visual observation indicates that these small fluctuations have little effect on the overall success of the center of energy cut.

While studying several parameters that relate to level 1 and level 2 trigger cuts, we observe that each aspect of our analysis of this proposed center of energy cut shows that it is a safe and effective method for separating signal events from background events at the level 2 trigger stage. The next step, discussed in the following chapter, is to find a way to implement this new cut within the limitations of the hardware designs of the boards in the DAQ system, using the flexibility of programmable chips installed on the boards.

Chapter 4

Center of Energy Implementation in the DAQ System

The Monte Carlo framework is designed to simulate, among other things, the energy signals from each detector channel. Having shown in the previous chapter that a center of energy cut is effective, the next step is to find a way to implement the calculation in the level 2 trigger system. The hardware at the level 2 trigger stage is fully capable of retrieving the energy information, but the firmware design needs to be modified to include the center of energy calculation in the ADC boards, the trigger boards, and the MACTRIS. Graduate student Jia Xu and associate researcher Monica Tecchio developed the firmware implementation and their work is summarized in this chapter.

4.1 CsI Energy and Position Readout

Before discussing the implementation of the center of energy cut in the firmware, we describe how the energy from the detector system is collected and digitized.

Each ADC board has sixteen channels, and each of these channels collects short samples of the energy present in a single detector component, such as a CsI crystal. The ADC boards run at 125 MHz and collect 64 samples per event, with 8 ns in between each sample. This means that the window for an event is approximately 500 ns, much larger than the width of the pulse; the full width at half maximum (FWHM) is expected to be about 60 ns. The incident pulse is actually much shorter, but the ADC boards have a special circuit that shapes and broadens the pulse.

The proportionally large window size allows us to identify accidental double events and coordinate timing differences between the different detectors. For example, the CsI trigger generally occurs after the veto trigger. In order to have both the CsI and veto triggers occur in the same window, we need to delay the veto trigger signal and have a window large enough to include both signals in the same time frame.

Noise from the photomultiplier tubes, pre-amplifiers, and within the ADC boards causes

a small amount of phantom energy to appear in most channels, so an algorithm in the ADC firmware studies the typical energy in each channel. This typical value, called a pedestal value, is assumed to correspond to zero energy and is subtracted from the incoming energy value for each sample. It will then send the result, if positive, or send zero if the result is negative, to a level 1 or level 2 trigger board.

ADC channels are mapped to specific crystals, and the location of each crystal is recorded in the firmware of the assigned ADC board. Combining the position and energy detected by each crystal, an ADC board can sum up the center of energy value for each 8ns sampling in the combined 16 channels. This value is formated into a hexadecimal string called a CoE word. The CoE word encodes information for three variables: E_T, the total energy sum; E_x, the center of energy along the x axis; and E_y, the center of energy along the y axis.

CoE words are attached to the data packets the ADC boards send to the level 2 trigger boards. The structure of the ADC packets, shown in figure 4.1, is the same whether the ADC board is communicating to a level 1 or level 2 trigger board and contains all the information the ADC board has for each of its crystals in a particular event. Each level 2 board uses the CoE words to calculate the E_T, E_x, and E_y for the combination of all the ADC boards connected to it, a sum involving the energies and positions of 256 CsI crystals. The original scheme for the level 2 trigger cut, where each level 2 board would search for a photon cluster over its set of 256 crystals, was inadequate because a cluster could easily be split between crystals mapped to different trigger boards, as shown in figure 1.4. The center of energy cut is possible to perform because the center of energy is nothing more than a sum of certain variables.

Figure 4.1 Structure of ADC Data Packets

As soon as the boards at the two edges of the level 2 crate have calculated the E_T, E_x, and E_y values for their respective crystals, those values are sent towards the MACTRIS board at the center of the crate via a daisy-chain signal, with each board adding its values to the sum. MACTRIS then calculates the center of energy radius for the entire crystal array, and makes a decision based on a predetermined threshold value.

If an event passes the center of energy cut, it is temporarily saved to an on-board memory module while waiting to be transferred to Mandolin. Level 2 boards have two 2Gb memories, each of which can store up to approximately 10,000 events. Level 2 boards write to one of the memories and simultaneously send out previously stored data from the other memory.

4.1.1 Peak Versus Integral of Gaussian Energy Signal

Given that the digitized signal from a CsI crystal has a gaussian waveform, there are two possible methods for finding the energy in a crystal. One option is to use the peak of the gaussian, which is expected to be proportional to the total energy; the other option is to

use the integral of the gaussian, which corresponds to the sum of the energies over all 64 samples in an event window. Jennifer Miller, an undergraduate in the Michigan K0TO group, studied the correlation between peak and total energy. This study concluded that the correlation between peak and total energy is not well established, so we currently use the integral calculation.

4.2 Firmware Implementation in Level 2 Trigger Boards

The firmware in the ADC and level 2 trigger boards was modified in order to calculate and transmit center of energy information. The center of energy calculation is completed in several steps. Figure 4.2 shows the data flow in the two programmable chips, Virtex 4 and Virtx 5, installed on each Level 2 trigger board.

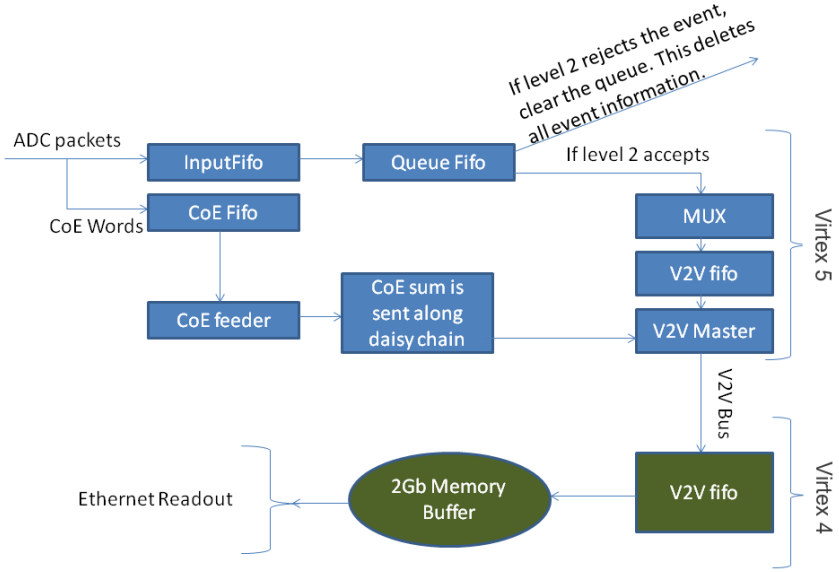

Figure 4.2 Data Flow In Firmware

MUX stands for multiplexer, which receives several channels simultaneously and turns them into a single stream of data. Fifo stands for "first in first out," which is a chronological ordered set of data, as opposed to traditional random access memory. Events in the fifo are processed in the order they arrive.

In order to implement the center of energy cut in the DAQ system, we needed to edit the ADC words to include an additional CoE word with center of energy information for 16 crystals, change the level 2 firmware to perform the center of energy calculation over 16 ADC boards, and change the MACTRIS firmware to find the overall center of energy

radius. Although the simulation studies in the previous chapter used 13 cm as an estimated threshold value, the precise threshold will be determined after more careful studies in the future, and the new value will then be programmed in the MACTRIS firmware. Even though the exact threshold is not yet known, the center of energy cut is ready for testing with live data in engineering runs, and, after a precise threshold is found, this new level 2 trigger cut will be used when the K0TO experiment turns on for its first physics during summer 2013.

Chapter 5

Conclusion

After completing a study of several parameters relating to a new level 2 trigger cut, we conclude that a trigger cut based on the center of energy in the CsI calorimeter is a safe and effective method for removing a large percentage of background events while retaining almost all signal events. A basic understanding of the characteristics of background events and the experimental setup indicated that such a cut might be useful, an expectation that was initially supported by an analysis of the center of energy distribution for a select set of background and signal events where all photons hit within a fiducial region of the CsI calorimeter. Further analysis of events that would have passed the level 1 veto cut show that the center of energy cut continues to be effective. An algorithm for performing the calculation has been implemented in the firmware, and this new level 2 trigger cut will be used when the K0TO experiment turns on for its first physics run in May 2013.

Bibliography

[1] A. Buras, M. Gorbahn, U. Haisch, and U. Nierste, "Charm Quark Contribution to K+ -> pi+ nu anti-nu at Next-to-Next-to-Leading Order," arXiv:hep-ph/0603079, Physical Review Letters 95 (2005).

[2] G. Isidori, F. Mescia, P. Paradisi, C. Smith, and S. Trine, "Exploring the flavour structure of the MSSM with rare K decays," arxiv:hep-ph/0604074 p. 3 (2006).

[3] M. Kobayashi and T. Maskawa, "CP Violation in the Renormalizable Theory of Weak Interactions," Progress of Theoretical Physics **49,** 652 (1973).

[4] B. et al., "Particle Data Group," Physical Review D 86 (2012).

[5] T.Inami and C.S.Lim, "Effects of Superheavy Quarks and Leptons in Low-Energy Weak Processes $K_L \to \mu\bar{\mu}$, $K^+ \to \pi^+ \nu\bar{\nu}$ and $K^0 \to \bar{K^0}$," Progress of Theoretical Physics **65,** 297 (1981).

[6] J. Brod, M. Gorbahn, and E. Stamou, "Two-loop electroweak corrections for the $K \to \pi\nu\bar{\nu}$ decays," Physal Review D 83, 034030 (2011).

[7] A. J. Buras, F. Schwab, and S. Uhlig, "Waiting for Precise Measurements of $K^+ \to pi^+ nunu$ and $K_L - > pi^0 nunu$," arXiv:hep-ph/0405132 (2004).

[8] F. Mescia, "The impact of rare K decays in New Physics searches," presented at CKM 2006, (Nagoya, Japan, December 2006).

[9] A. et al, "Experimental study of the decay $K_L^0 \to \pi^0 \nu\bar{\nu}$," Physical Review D 81 (2010).

[10] T. Yamanaka and the K0TO Collaboration, "Proposal for $K_L \to \pi^0 \nu\bar{\nu}$ Experiment at J-PARC," (2006).

[11] J. Xu, "Private communication," .